Perforin activity at membranes leads to invaginations and vesicle formation

Tilen Praper[a,1], Andreas F.-P. Sonnen[b,1,2], Aleš Kladnik[a], Alberto O. Andrighetti[c,d], Gabriella Viero[c], Keith J. Morris[e], Emanuela Volpi[e], Lorenzo Lunelli[c], Mauro Dalla Serra[c], Christopher J. Froelich[f], Robert J. C. Gilbert[b,3], and Gregor Anderluh[a,3,4]

[a]Department of Biology, Biotechnical Faculty, University of Ljubljana, Večna pot 111, 1000 Ljubljana, Slovenia; [b]Division of Structural Biology, Wellcome Trust Center for Human Genetics, University of Oxford, Roosevelt Drive, Oxford OX3 7BN, United Kingdom; [c]National Research Council Institute of Biophysics and Bruno Kessler Foundation, via alla Cascata 56/C, 38123 Trento, Italy; [d]Department of Physics, University of Trento, via Sommarive 14, 38123 Trento, Italy; [e]Wellcome Trust Center for Human Genetics, University of Oxford, Roosevelt Drive, Oxford OX3 7BN, United Kingdom; and [f]Department of Medicine, NorthShore University Health System Research Institute, Evanston, IL 60201

Edited by Ari Helenius, Swiss Federal Institute of Technology, Zurich, Switzerland, and approved October 20, 2011 (received for review May 14, 2011)

The cytotoxic cell granule secretory pathway is essential for immune defence. How the pore-forming protein perforin (PFN) facilitates the cytosolic delivery of granule-associated proteases (granzymes) remains enigmatic. Here we show that PFN is able to induce invaginations and formation of complete internal vesicles in giant unilamellar vesicles. Formation of internal vesicles depends on native PFN and calcium and antibody labeling shows the localization of PFN at the invaginations. This vesiculation is recapitulated in large unilamellar vesicles and in this case PFN oligomers can be seen associated with the necks of the invaginations. Capacitance measurements show PFN is able to increase a planar lipid membrane surface area in the absence of pore formation, in agreement with the ability to induce invaginations. Finally, addition of PFN to Jurkat cells causes the formation of internal vesicles prior to pore formation. PFN is capable of triggering an endocytosis-like event in addition to pore formation, suggesting a new paradigm for its role in delivering apoptosis-inducing granzymes into target cells.

Pathogen-infected and tumor cells are eliminated through granule-mediated apoptosis. Perforin (PFN), which is secreted together with proteases (granzymes) from cytotoxic T lymphocytes or natural killer cells, has a central role in this process, aiding the intracellular delivery of granzymes to initiate apoptosis of target cells (1, 2). Two models are currently available for the function of PFN. The first involves formation of stable plasma membrane pores that allow the direct transfer of granzymes into the target cell, which are later removed by membrane repair (1, 3, 4). This model is based primarily on visualization of pore-like structures on the membrane of the target cells (5–7). The other model, originally postulated by Podack and coworkers, proposes that the delivery process requires endocytosis of both PFN and granzyme, with the protease subsequently being released to the cytosol (4, 8).

Mature PFN is a 533 residue protein consisting of three domains: an N-terminal membrane attack complex/perforin (MACPF) domain, an intervening EGF-like domain, and a C-terminal calcium-binding C2 domain, which is responsible for the initial Ca^{2+}-dependent binding of PFN to membrane surfaces (9–11). The structures of PFN and other MACPF domain proteins (12–15) reveal they have folds related to those of the cholesterol-dependent cytolysins (CDCs) of Gram-positive bacteria, such as pneumolysin from *Streptococcus pneumoniae* (16–19). These observations suggest that the effects of PFN and other MACPF proteins on membranes derive from a mechanism related to the CDCs, which involves membrane binding and oligomerization to large arc or ring structures. MACPF/CDC domains refold into membrane-inserted pore forms via an oligomeric prepore state; both prepore and pore states have been observed for PFN (15, 20, 21). It has been argued CDCs form pores as full ring-shaped oligomers and as arcs (17, 22); a recent study by us supports this view for PFN (20, 21) in agreement with a simultaneous cell biology study (23).

The binding of proteins to lipid membranes may affect the curvature of the bilayer, producing invaginations (24, 25) or inducing the formation of intraluminal vesicles (ILVs) (26, 27). This phenomenon is thought to derive from insertion of protein into one monolayer, creating tension relieved by bending of the membrane (28, 29). Inserted regions of proteins may be α-helical as in epsin (30) or the hydrophobic amino acids of a C2 domain as in synaptotagmin (31). Many protein domains that modify membrane curvature are dimeric (31, 32), or oligomerize or cluster (24, 33) to induce invaginations. Because PFN contains a membrane-binding C2 domain that could affect the chemicophysical properties of the membrane and has also a tendency to aggregate on membranes (11, 34, 35), we studied whether PFN might alter membrane dynamics apart from pore formation. This reassessment was also prompted by the fact that formation of vesicles has been associated with the action of PFN on cells (2, 3, 23, 36, 37).

In the present study we used a variety of biophysical and imaging techniques to investigate the effects of PFN on several model membrane systems with different intrinsic curvatures and on live cells. As well as pore formation in giant unilamellar vesicles (GUVs) (20) we found that PFN is able to induce invaginations and ILV formation in GUVs and large unilamellar vesicles (LUVs) and further confirmed the membrane remodeling capacity of PFN on a planar lipid membrane (PLM). Invaginations and ILVs in GUVs contain the surrounding medium. In living human cells PFN induced invaginations and vesiculation prior to pore formation and without ATP dependence; other pore-forming proteins did not. Thus the membrane infolding we observe can be specific to PFN. These findings suggest how PFN could directly induce cell entry of granzymes via endosomes from which their pore-mediated release would occur (23, 37).

Author contributions: T.P., A.S., M.D.S., R.J.C.G., and G.A. designed research; T.P., A.S., A.K., A.O.A., G.V., K.J.M., E.V.V., L.L., M.D.S., C.F., R.J.C.G., and G.A. performed research; T.P., A.S., M.D.S., R.J.C.G., and G.A. contributed new reagents/analytic tools; T.P., A.S., A.K., A.O.A., G.V., K.J.M., E.V.V., L.L., M.D.S., R.J.C.G., and G.A. analyzed data; and T.P., A.S., M.D.S., C.F., R.J.C.G., and G.A. wrote the paper.

The authors declare no conflict of interest.

This article is a PNAS Direct Submission.

[1]T.P. and A.S. contributed equally to this work.

[2]Present address: Center of Chronic Immunodeficiency, University of Freiburg, Breisacher Strasse 117, 79106 Freiburg, Germany.

[3]To whom correspondence may be addressed. E-mail: gregor.anderluh@ki.si or gilbert@strubi.ox.ac.uk.

[4]Present address: National Institute of Chemistry, Hajdrihova 19, 1000 Ljubljana, Slovenia.

This article contains supporting information online at www.pnas.org/lookup/suppl/doi:10.1073/pnas.1107473108/-/DCSupplemental.

Results

We have recently shown that PFN enables rapid pore-mediated influx of low molecular weight fluorescent dextran (FITC-labeled dextran 4000, D4) into GUVs while they remain impermeable to high molecular weight dextran (FITC-dextran 70000, D70) (20). We noted that a significant fraction of GUVs (~30–40%) possess invaginations and/or ILVs (i.e., separated invaginations; Fig. 1*A*). We therefore measured the diameter of GUVs and found the average size of GUVs decreased in the presence of PFN compared to its absence (Fig. S1) with significantly more GUVs of 10–20 μm diameter. In all cases, the invaginations started to form rapidly and it was not possible to image their early stages in GUVs; more mature invaginations and ILVs then formed within minutes (Fig. 1*B*). In the absence of PFN only 1.3% of GUVs observed showed ILVs. We also noted that first the membrane invaginations and then the ILVs were filled with the fluorescent dextrans, irrespective of the size of the dextran added to the surrounding medium [D4, FITC-labeled dextran 10000 (D10) or D70; Fig. 1 *B* and *C*]. Pores capable of transmitting D4 formed in the GUV outer membrane but not pores allowing the passage of D10 or D70 (Fig. 1*C*). The reduced permeabilization for larger dextrans suggests that the passage of granzyme through pores associated with the GUV exterior might be rather slow. In agreement we showed that GUVs imaged with fluorescent GzmB in the presence of PFN showed no entry at 10 min, whereas passage of the GzmB into ILVs was completed by 5 min (Fig. S2). Quite often more than one ILV was formed within a single GUV (Fig. 1 *B–D*), suggesting focal action of the exogenous PFN. Three-dimensional (3D) reconstitution indicated that the ILVs were complete and in some cases separated from the originating membrane (Fig. 1 *C* and *D*). The GUVs used here are a simple model system consisting only of pure lipids so to check whether the same phenomenon occurs in a more complex model system we prepared GUVs from erythrocyte membranes. Such GUVs resemble the plasma membrane of target cells because their membranes consist of a heterogeneous mixture of native lipids as well as integral and peripheral membrane proteins. As with the GUVs of defined lipid composition, PFN shows Ca^{2+}-dependent binding in surface plasmon resonance experiments employing immobilized erythrocyte ghosts as the ligand (Fig. S3*A*). Similarly, PFN was also able to induce the formation of ILVs in GUVs prepared from erythrocyte membranes (Fig. S3*B*).

Because GUVs are extremely sensitive to any chemical or physical changes in the surrounding medium (38–40), we performed a number of controls to show that the effects we observe are due to the presence of functional PFN. First, ILV formation was clearly dependent on the presence of calcium; as in the absence of PFN, we observed significantly less invaginations and ILVs in the absence of Ca^{2+} (Fig. 1*E*). Thus interaction of PFN with the lipid membranes of GUVs is the underlying reason for ILV formation; the extent of ILV formation was dependent on the concentration of PFN and the incubation time and did not proceed when PFN was replaced by bovine serum albumin (Fig. 1*F*). We then excluded osmotic effects as the cause of ILV formation. An osmotic imbalance between the surrounding medium and the GUV lumen could be caused by the buffer in which PFN was isolated and that was added together with the protein to the GUVs. Without PFN this buffer induced negligible ILV formation (Fig. 1*E*) and incubation of GUVs with heat-denatured PFN did not induce ILV formation (Fig. 1*F*). This experiment provides

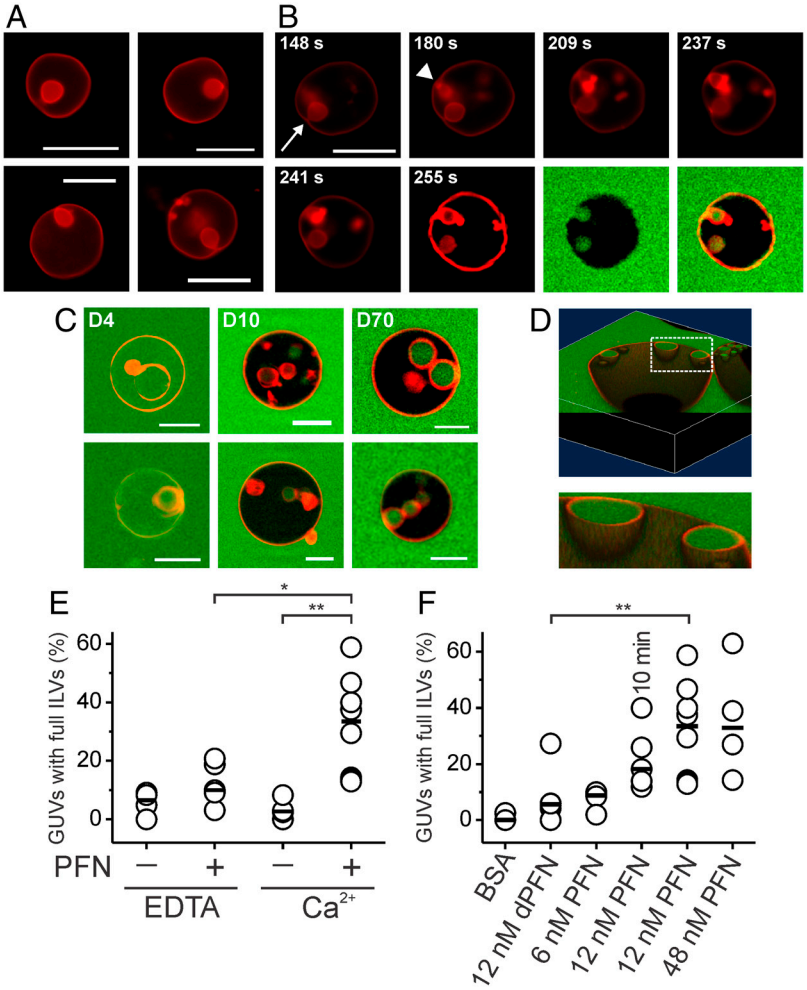

Fig. 1. Formation of invaginations and ILVs in GUVs by PFN. (*A*) Invaginations and secondary vesicle formation induced by 12 nM PFN in the presence of 0.1 mM Ca^{2+}. The fluorescence derived from rDHPE is shown in red. (*B*) Time course of PFN-induced secondary vesicle formation. The formation of two invaginations on a single GUV may be seen, denoted by an arrow and an arrowhead. rDHPE fluorescence (red), D70 fluorescence (green), and a merged image is shown for the final image. The time (in seconds) after the mixing of all components is shown on each image. (*C*) Secondary vesicles are filled with external medium that contains fluorescent probes as indicated. For D4 also the primary GUV is full, because PFN pores formed on the membranes allow the passage of this small dextran across the membrane. (*D*) Three-dimensional reconstitution of GUVs with secondary vesicles. D70 was in the external medium. The indicated area is shown enlarged below. (*E–F*) Experiments were performed in the presence of 70 kDa FITC-labeled dextran, 12 nM PFN, and the amount of GUVs with secondary vesicles was quantified after 45 min, except as indicated. In total four to eight independent experiments were performed for each condition with 104–211 GUVs analyzed. Different conditions were compared with a nonparametric Mann–Whitney test (*, $p < 0.05$; **, $p < 0.01$; n.s., not significant). (*E*) Experiment was performed in the presence of 5 mM EDTA or 0.25 mM $CaCl_2$, as indicated. The buffer used for the purification of PFN was used as a control in the absence of PFN. Each data point represents an independent experiment, the median is shown by the black line. (*F*) PFN concentration dependence of ILV formation. Experiments that were performed in the presence of 6, 12, or 48 nM PFN are compared to the bovine serum albumin control (12 nM) and control where PFN (12 nM) was denatured with heat (dPFN). Quantification of ILVs was done for 12 nM PFN also after 10 min as indicated.

the most appropriate control, as all the components in the solution added were the same save for the lack of PFN activity. Another source for osmotic imbalance could also be the fluorescent dextrans that were used for imaging at up to submillimolar concentrations (the highest used concentration was 0.1 mM for D4). However, several observations excluded the presence of dextrans as a possible reason for ILV formation. First, we see invaginations also in the absence of dextrans (Fig. 1*A*). Next, if the presence of dextrans causes significant osmotic imbalance, then the formation of invaginations and ILVs should be dependent on the size of the dextrans, as smaller dextrans would rapidly equilibrate across the pores (20) and not exert an osmotic pressure on the membrane (larger dextrans cannot equilibrate and, consequently, more ILVs should be observed). However, the amount of ILVs was independent of the size of the dextran used—in all cases we observed that approximately 30% of GUVs incubated with PFN possess ILVs filled with dextran (Fig. S4*A*). Finally, we also performed the reverse experiment, by encapsulating fluorescent dextran in the GUV lumen while the surrounding medium was devoid of the probe. In this case the osmotic pressure should work in the other direction and would, in principle, prevent the formation of ILVs and perhaps even cause increased blebbing. However, we also observed formation of ILVs in this instance (Fig. S4*B*).

To independently assess that PFN is bound to GUVs in these conditions and to check whether it is located at the vesiculation sites, we visualized PFN on the surface of GUVs with δG9-Alexa-labeled antibody. GUVs were stained only in the presence of PFN (Fig. 2 *A* and *B*; Fig. S5*A*), but not in its absence (Fig. 2*C*) or when an isotope antibody control was used (Fig. 2*D*). We noted that the staining was not homogeneous, but appeared to be concentrated at the necks and around the interior of the invaginations, which are nascent ILVs (Fig. 2*B*). This clustering of PFN seemed to occur whether the GUVs were flaccid or tense (Fig S5*A*) and could be further shown using atomic force microscopy in which arc and ring structures formed by PFN on the membrane surface were clearly observed (Fig. S5*B*).

Addition of PFN to LUVs for periods of 0.1–5 min also revealed the evolution of discrete internal membrane compartments from invaginations pinched away from a resealed outer membrane (Fig. 2*E*). In addition to transmembrane pores previously characterized (20) we also observed structures resembling PFN oligomers (rings and/or arcs) associated with the necks of invaginating LUVs (Fig. 2*E*). This observation suggests a mechanism by which PFN could convert invaginations into ILVs as pore formation at the neck might well lead to separation of the lower invagination from the upper outer membrane. This mechanism would be an inverted form of the membrane fusion enabled by cellular and viral fusion proteins. However, adding buffer alone we also observed that invaginations occurred in LUVs in the absence of PFN—most likely due to osmotic effects and the high curvature of their bilayers compared to those in GUVs (see *SI Materials and Methods*). We further investigated by image analysis of 252 images in which PFN oligomers could be seen directly associated with the necks between primary LUVs and invaginations (as in Fig. 2*E*), compared to analysis of 109 similar invagination necks in the absence of PFN. A superstructure is present above the invaginations in the presence of PFN (Fig. 2*F*) but not in its absence (Fig. 2*G*). The shape of this crown-like structure is very similar to the previously observed PFN prepore oligomer (20) (Fig. 2*F*), suggesting that the equivalent presence of PFN in invaginating GUVs has a role in the maturation of invaginations to ILVs because above we have shown the formation of such invaginations to be PFN dependent. Contour plots allow a quantitative comparative assessment of the density levels at either side of the visualized membrane boundaries (Fig. 2 *F* and *G*): Apart from the oligomeric structure atop the invagination junction, bound PFN is apparent around its inner surface as the relative, class-average-based electron density level is clearly higher on the inside of the PFN-containing invagination

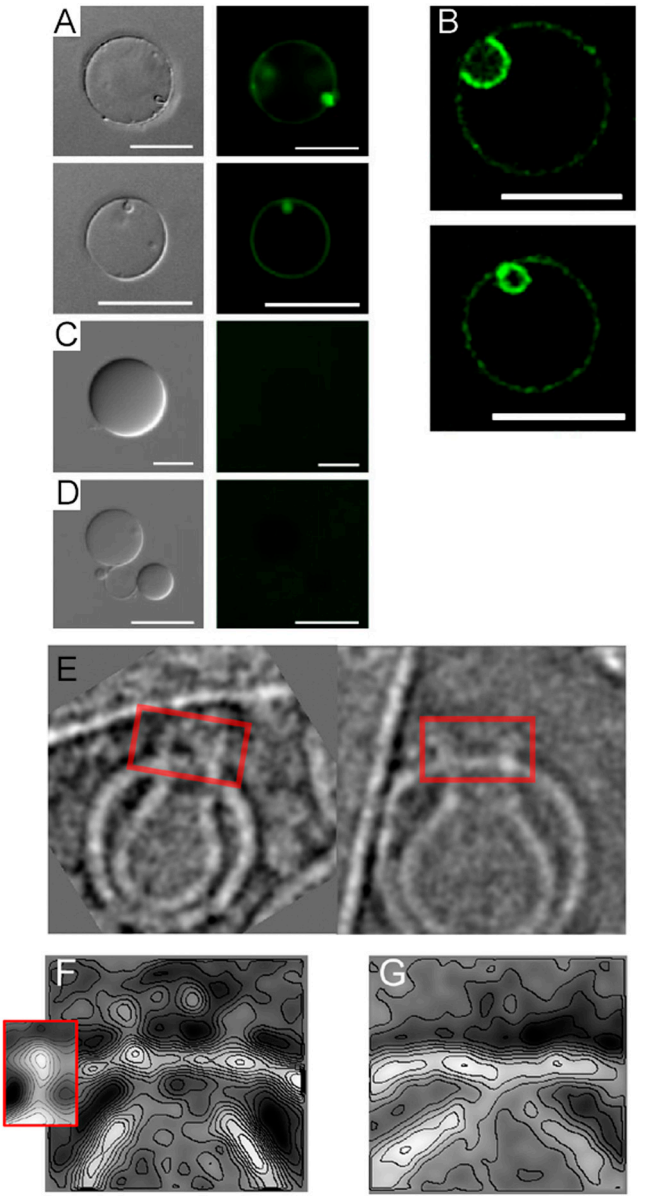

Fig. 2. Detection of membrane-bound PFN by anti-PFN δG9-FITC labeled antibodies and cryo-EM. (*A*) Fluorescence microscopy of GUVs in the presence of 12 nM (*Top*) or 24 nM (*Bottom*) of PFN stained with anti-PFN δG9-FITC labeled antibodies. (*B*) Confocal microscopy that shows a cross section of two GUVs with enriched signal in the invagination (*Top*) and in the ILV (*Bottom*). The experiment was performed as in *A*, the concentration of PFN was 24 nM. (*C*) GUVs in the absence of PFN and in the presence of anti-PFN δG9-FITC labeled antibodies. (*D*) GUVs in the presence of 24 nM PFN and isotype antibodies control (IgG2b isotype; antiglycophorin-FITC labeled antibodies). Scale bar is 20 μm in *A*, *B*, and *D*, but 10 μm in *C*. The concentration of antibodies was approximately 30 μg/mL. Differential interference contrast images are shown for comparison (*Left*). (*E*) Images of LUV invaginations with PFN oligomers (boxed). (*F*) Representative class average contour plot derived from alignment and classification of images of the junctions between primary outer membranes and secondary internal compartments/invaginations in the presence of PFN. *Inset* shows the subunit structure of PFN in its oligomeric prepore state bound to the membrane surface (20). (*G*) The equivalent image to *F* derived in the absence of PFN.

when compared to that obtained without PFN. The binding of PFN to invaginating membranes suggests it could directly induce such in-curving of the lipid bilayer, perhaps through oligomerization (see *Discussion*).

To further assess lipid bilayer remodeling by PFN, we took a PLM approach in which, akin to the GUV system, the bilayer is

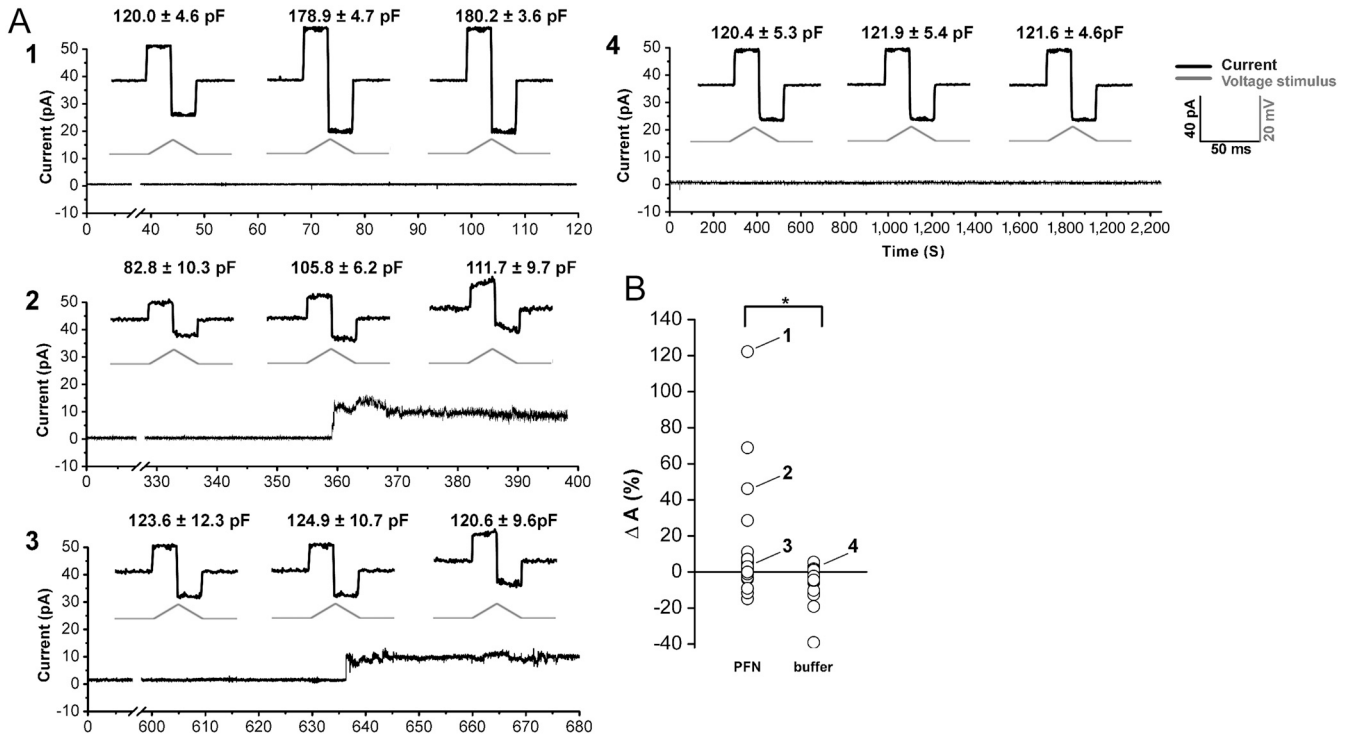

Fig. 3. PFN induces changes in membrane area in PLM. (*A*) Representative traces of electrical current for experiments 1–4 highlighted in *B*. The current response from which the capacitance was calculated is enlarged, the triangular wave form of voltage is shown below the enlarged response (gray). The calculated capacitance shown above the trace is the average of 10 measurements on the same time interval ±standard deviation. The scale for all enlargements is identical (40 pA, 50 ms, 20 mV). The current was measured at a constant voltage of +10 mV with the exception of intervals where the triangular wave form were applied (those intervals were removed from the main current trace for the clarity). (*B*) Changes in membrane area (ΔA) in the presence of PFN or buffer (39 or 41 measurements on freshly prepared membranes, respectively). We calculated ΔA from the membrane C_m as described in *Materials and Methods*.

essentially flat with the same packing characteristics between the two lipid leaflets [in the LUV system membrane curvature is much greater and packing asymmetry between leaflets can result in membrane defects (41)]. Such a lipid membrane is a condenser of parallel plates and thus variation in the membrane area causes change in the membrane capacitance (see *SI Materials and Methods*). Reliable measurement of the membrane capacitance is impossible in the presence of high currents, e.g., large membrane pores, so we limited our investigations to experiments where there were no or only small PFN pores. The addition of PFN to a solution bathing a stable preformed bilayer induced an increase in membrane capacitance both without pores (Fig. 3*A*, trace 1) and with only small pores (Fig. 3*A*, trace 2); pore formation also occurred in the absence of capacitance changes (Fig. 3*B*, trace 3) and we thus think membrane invagination is not directly associated with pore formation. In the absence of PFN the electrical parameters of the lipid membrane (i.e., current and capacitance) remain stable for hours (Fig. 3, trace 4); only on the introduction of PFN do they change. The PLM data are thus consistent with the ability of PFN, even at non-pore-forming concentrations, to induce an increase in membrane area, i.e., an invagination.

We studied PFN's induction of vesiculation in living Jurkat cells stained to highlight the cell membrane and with the fluorescent nucleic acid dye SYTOX Green in the surrounding medium (see *Materials and Methods*). We added a small volume of PFN and observed membrane infolding and vesiculation prior to SYTOX Green cell entry (Fig. 4*A*, Fig. S6, Movies S1 and S2). In repeating the experiment we first diluted the PFN in a Ca^{2+}-free buffer before mixing with an equal volume of cells in a 1.25 mM Ca^{2+}-containing buffer, to ensure adequate mixing (see *Materials and Methods*), and controlled for the phenomenon being due to active PFN by repeating the experiment with EDTA, and adding the pore-forming proteins pneumolysin or lysenin from *Eisenia foetida* (Fig. 4 *B–E*, Movies S3, S4, S5, S6, S7, S8, S9, and S10). PFN induced infolding of the Jurkat cell membrane prior to cellular SYTOX Green staining (Fig. 4*B*, Movies S3 and S4). EDTA prevented membrane infolding and pore formation (Fig. 4*C*, Movies S5 and S6), pneumolysin produced blebbing of membranes outward—the opposite phenomenon to PFN (Fig. 4*D*, Fig. S3 for close-up, Movies S7 and S8)—and lysenin, a pore-forming toxin forming small pores (42), caused no change in membrane structure except for a slight osmotic rounding (Fig. 4*E*, Movies S9 and S10). The ability of pneumolysin to cause blebbing has been documented before (43). We also used rotenone (inhibiting mitochondrial complex I) or azide (inhibiting complex IV) (see *SI Materials and Methods*) to show that ATP depletion does not prevent PFN-induced vesiculation (Movies S11, S12, S13, and S14). These data indicate that PFN is capable of inducing membrane restructuring in living eukaryotic cells similar to that observed in GUVs and LUVs. Vesiculation is prior to pore formation and is to be contrasted with pneumolysin-induced blebbing, and only small pores formed by lysenin. Hence, PFN is capable of directly inducing vesiculation in living cells.

Discussion

Cell-mediated immune cytotoxicity relies on PFN-triggered delivery of apoptosis-inducing granzymes to eliminate virus-infected or tumor cells (1, 2). Here we show that native human PFN is capable of changing the morphology of lipid membranes to give invaginations and ILVs, as well as pore formation in three different model membrane systems and also in living cells.

Results of several studies highlight the ability of eukaryotic, prokaryotic, or virus proteins, e.g., endophilin 1 (44), endosomal sorting complex (26, 27), shiga toxin (24), matrix protein of vesicular stomatitis virus (45), SV40 and VP1 (25), and antimicrobial peptides (46) to modulate membrane curvature and induce internalization or externalization independent of cellular endocytotic mechanisms or external sources of energy (endophilin produces

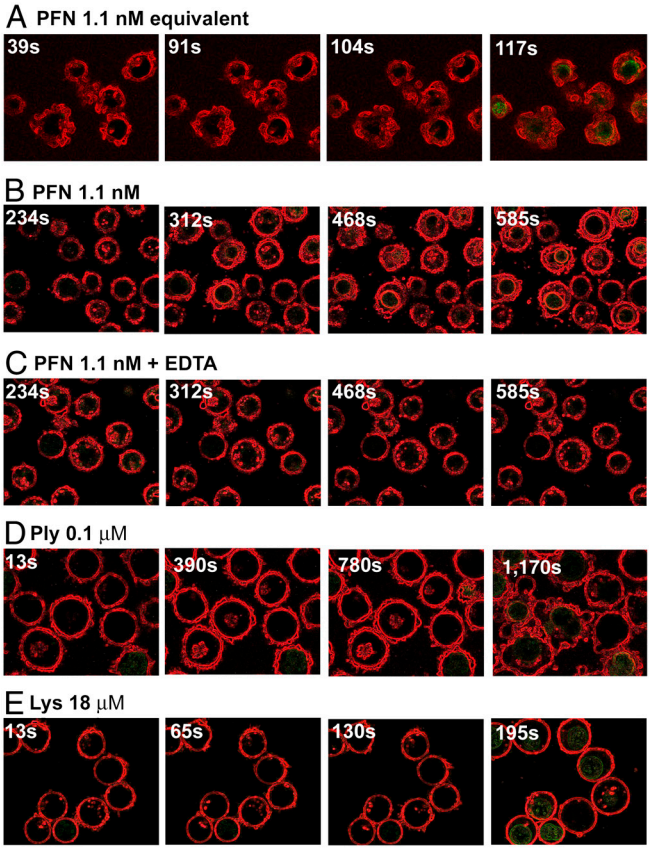

Fig. 4. Jurkat cells under permeabilization, Membranes have been stained red with CellMask PM Orange (Invitrogen) and the green dye is SYTOX Green (Invitrogen). The time in seconds at which each image was taken is given at the top left in each case. These images have been edged-enhanced using ImageJ (http://imagej.nih.gov/ij/index.html) software; the full movies of unenhanced and enhanced data are presented as Movies S1, S2, S3, S4, S5, S6, S7, S8, S9, and S10. (*A*) Final concentration of PFN is 1.1 nM; (*B*) 1.1 nM final concentration, a positive control for *C*; (*C*) 1.1 nM in the presence of 2 mM EDTA. (*D*) Pneumolysin concentration is 0.1 μM; (*E*) 18 μM lysenin.

exvagination, the others cause invaginations). The remarkable capability of certain proteins and viruses to induce formation of membrane invaginations has also been confirmed by computer simulations (47, 48). Individual protein-protein and protein-membrane interactions are too weak to cause large-scale changes in membrane geometry so the cooperative action of many protein molecules is essential (47). We noticed that invaginations were present mostly on more convoluted GUVs (Fig 1*A*), which are the consequence of PFN pores (20), and observed a high density of PFN molecules on the invaginations. These observations agree with the idea that invagination and ILV formation is largely controlled by tension-dependent energy at the invagination neck and the density of the proteins bound on the membrane (25). A remaining puzzle is why exvaginations are not seen—even when the osmotic pressure is weighted in their favor (Fig. S4*B*); a prerequisite is asymmetry in the interaction of PFN with the membrane. The preferential formation of invaginations could be an effect of PFN itself or of Ca^{2+} at the exterior face of the bilayer, perhaps involving the induction by PFN of rigidity or steric constraints making curvature outward disfavored. A possible mechanism, in agreement with simulation data (47), is the insertion of PFN into the upper leaflet of the bilayer at its C2 domain, coupled with oligomerization. Atomic force microscopy imaging shows PFN oligomers on GUV membranes and these could induce a bulging inward to initiate unidirectional vesiculation, further maintained by the geometry of the inserted PFN in agreement with the data presented in Fig. 2. The homologous protein pneumolysin is known to alter membrane curvature via its membrane-binding domain (49). Such a modification in lateral lipid order and microdomain structure has been observed and modeled for cholera toxin binding, and argued to present a plausible origin for clathrin-independent vesicle formation (48).

Our results suggest that PFN has the ability to stimulate formation of endocytic vesicles allowing entry of fluid-phase or membrane-bound molecules into the cell. This process may be influenced by remodeling of membranes by phenomena such as clathrin binding, cytoskeletal dynamics, and dynamin scission, though in the GUV system, at least, PFN appears sufficient and in the PLM system it is independent of pore formation. In contrast, SV40 and its protein VP1 are able to form invaginations on GUVs, but scission to form ILVs depends on signal transduction and active cellular scission mechanisms (25). Our data lend support to a variant of the endosomolysis model (2, 8) in which initial endocytosis of granzymes is a function of PFN as well as subsequent cytosolic delivery from the endosome mediated by the larger PFN pores (20, 23). As shown by our antibody labeling and cryo-EM, PFN is associated with the invaginated membrane neck. This localization suggests the possibility of two effects of PFN—the promotion of membrane infolding and the maturation of invaginations into ILVs. PFN thus appears to promote a unique form of endocytosis that begins with an initial interaction with the membrane, rather than a receptor-mediated transmembrane signal or Ca^{2+} stimulation through a transmembrane pore. Large endosomes have been observed after treatment of HeLa cells with sublytic concentrations of PFN (36, 37); these gigantosomes were an order of magnitude larger in diameter than normal endosomes and were filled with 70 kDa fluorescent dextran (37). A more recent study (23) has shown that PFN forms functional pores of variable diameter and stability in the plasma membrane and endosomal membrane, exactly in agreement with insights presented here as well as previously (20). The transient (23), small, and unstable (20) pores formed in the plasma membrane may assist in triggering endocytosis or may be side effects of PFN's role in it. It was also shown that PFN clusters on the gigantosomes (23) just as it is shown here to cluster on the GUV's invaginated vesicles: the larger pores in the gigantosomes presumably deliver GzmB to the cytosol. Our work therefore takes insights to date to a unique level, as we observe the formation of vesicles within Jurkat cells treated with PFN over a very short timescale (Fig. 4*A*) consistent with identical phenomena occurring in GUVs and Jurkat cells. It seems that the scale of PFN-mediated membrane infolding is determined by the size and the structural characteristics of the membrane being targeted; GUVs form the largest ILVs, on Jurkat cells vesicles of intermediate size are formed, and ILVs derived from LUVs have the smallest diameter. Thus, we suggest that the capacity of PFN to induce invagination and vesiculation is the reason why the endosomes formed in live cells when challenged by purified PFN or by natural killer cells are so large (23, 37); which would also explain how gigantosome formation starts in the absence of receptor protein-triggered coated pit formation. In cells, PFN's unique form of receptor-independent endocytosis is most likely assisted by the recruitment of clathrin to the curved inner face of the invagination so that their synergy generates the gigantosomes (23).

In summary, our investigations highlight the complex nature of the interaction of PFN with lipid membranes. Our data suggest that the function of PFN at target membranes is not limited to pore formation alone but includes the facilitation of endocytosis.

Materials and Methods

Materials. Native human PFN was isolated as described by Froelich et al. (50) (Fig. S7). Pneumolysin was purified according to Gilbert et al. (51) and lysenin according to Bruehn et al. (52). For other reagents see *SI Materials and Methods*.

Electroformation of GUVs. GUVs were prepared by electroformation as described (53) with modifications (see *SI Materials and Methods*).

GUV Imaging Using Fluorescence Microscopy. GUVs mixed with PFN and fluorescent dextran were imaged by grid-confocal microscopy or by confocal laser-scanning microscopy (see *SI Materials and Methods*).

Cryo-EM. LUVs mixed with PFN were flash-frozen in liquid ethane and imaged using an FEI F30 FEG cryoelectron microscope (see *SI Materials and Methods*).

Planar Lipid Bilayer Experiments and Membrane Area Measurements. Solvent-free PLMs were formed as described (54). Nanomolar PFN was added to the *cis* side of a preformed bilayer. Membrane capacitance was then measured alongside pore formation (see *SI Materials and Methods*).

Live Cell Imaging. Jurkat cells were stained with CellMask PM Orange and SYTOX Green and imaged using an Axiovert 200M microscope on a Zeiss 510 MetaHead laser-scanning confocal system (see *SI Materials and Methods*).

ACKNOWLEDGMENTS. We thank Dr. Janja Majhenc and Vesna Arrigler for the help with the GUV electroformation, Miha Mikelj for the help with the giant unilamellar vesicles experiments and Dr. Mojca Benčina for the help with the confocal microscopy. R.J.C.G. is a Royal Society University Research Fellow. C.J.F. was supported through National Institutes of Health Grant 5R01AI04494-03. A.S. held a Wellcome Trust four-year DPhil Studentship in Structural Biology and the Center of Chronic Immunodeficiency and is supported by the German Bundesministerium für Bildung und Forschung. T.P. and G.A. received financial support from the Slovenian Research Agency. T.P. was supported by the Federation of the Societies of Biochemistry and Molecular Biology Collaborative Experimental Scholarship for Central and Eastern Europe and a fellowship provided by the Slovene Human Resources Development and Scholarship Fund. The collaboration between R.J.C.G. and G.A. was supported in part by a Royal Society International Joint Project grant and an European Molecular Biology Organization Short term fellowship. The collaboration between M.D.S. and G.A. was partly supported by the Italy-Slovenia bilateral project. The financial support of INSTRUCT (http://www.structuralbiology.eu/) is also gratefully acknowledged.

1. Bolitho P, Voskoboinik I, Trapani JA, Smyth MJ (2007) Apoptosis induced by the lymphocyte effector molecule perforin. *Curr Opin Immunol* 19:339–347.
2. Pipkin ME, Lieberman J (2007) Delivering the kiss of death: Progress on understanding how perforin works. *Curr Opin Immunol* 19:301–308.
3. Voskoboinik I, Smyth MJ, Trapani JA (2006) Perforin-mediated target-cell death and immune homeostasis. *Nat Rev Immunol* 6:940–952.
4. Metkar SS, et al. (2002) Cytotoxic cell granule-mediated apoptosis: Perforin delivers granzyme B-serglycin complexes into target cells without plasma membrane pore formation. *Immunity* 16:417–428.
5. Podack ER, Dennert G (1983) Assembly of two types of tubules with putative cytolytic function by cloned natural killer cells. *Nature* 302:442–445.
6. Young JD, Hengartner H, Podack ER, Cohn ZA (1986) Purification and characterization of a cytolytic pore-forming protein from granules of cloned lymphocytes with natural killer activity. *Cell* 44:849–859.
7. Young LH, et al. (1990) Perforin-mediated myocardial damage in acute myocarditis. *Lancet* 336:1019–1021.
8. Froelich CJ, et al. (1996) New paradigm for lymphocyte granule-mediated cytotoxicity. Target cells bind and internalize granzyme B, but an endosomolytic agent is necessary for cytosolic delivery and subsequent apoptosis. *J Biol Chem* 271:29073–29079.
9. Uellner R, et al. (1997) Perforin is activated by a proteolytic cleavage during biosynthesis which reveals a phospholipid-binding C2 domain. *EMBO J* 16:7287–7296.
10. Voskoboinik I, et al. (2005) Calcium-dependent plasma membrane binding and cell lysis by perforin are mediated through its C2 domain: A critical role for aspartate residues 429, 435, 483, and 485 but not 491. *J Biol Chem* 280:8426–8434.
11. Praper T, et al. (2010) Human perforin permeabilizing activity, but not binding to lipid membranes, is affected by pH. *Mol Immunol* 47:2492–2504.
12. Hadders MA, Beringer DX, Gros P (2007) Structure of C8alpha-MACPF reveals mechanism of membrane attack in complement immune defense. *Science* 317:1552–1554.
13. Rosado CJ, et al. (2007) A common fold mediates vertebrate defense and bacterial attack. *Science* 317:1548–1551.
14. Slade DJ, et al. (2008) Crystal structure of the MACPF domain of human complement protein C8 alpha in complex with the C8 gamma subunit. *J Mol Biol* 379:331–342.
15. Law RH, et al. (2010) The structural basis for membrane binding and pore formation by lymphocyte perforin. *Nature* 468:447–451.
16. Anderluh G, Lakey JH (2008) Disparate proteins use similar architectures to damage membranes. *Trends Biochem Sci* 33:482–490.
17. Gilbert RJ (2005) Inactivation and activity of cholesterol-dependent cytolysins: What structural studies tell us. *Structure* 13:1097–1106.
18. Rosado CJ, et al. (2008) The MACPF/CDC family of pore-forming toxins. *Cell Microbiol* 10:1765–1774.
19. Rossjohn J, Feil SC, McKinstry WJ, Tweten RK, Parker MW (1997) Structure of a cholesterol-binding, thiol-activated cytolysin and a model of its membrane form. *Cell* 89:685–692.
20. Praper T, et al. (2011) Human perforin employs different avenues to damage membranes. *J Biol Chem* 286:2946–2955.
21. Metkar SS, et al. (2011) Perforin rapidly induces plasma membrane phospholipid flip-flop. *PLoS One* 6:e24286.
22. Tweten RK (2005) Cholesterol-dependent cytolysins, a family of versatile pore-forming toxins. *Infect Immun* 73:6199–6209.
23. Thiery J, et al. (2011) Perforin pores in the endosomal membrane trigger the release if endocytosed granzyme B into the cytosol of target cells. *Nature Immunol* 12:770–777.
24. Romer W, et al. (2007) Shiga toxin induces tubular membrane invaginations for its uptake into cells. *Nature* 450:670–675.
25. Ewers H, et al. (2010) GM1 structure determines SV40-induced membrane invagination and infection. *Nat Cell Biol* 12:11–18.
26. Wollert T, Wunder C, Lippincott-Schwartz J, Hurley JH (2009) Membrane scission by the ESCRT-III complex. *Nature* 458:172–177.
27. Wollert T, Hurley JH (2010) Molecular mechanism of multivesicular body biogenesis by ESCRT complexes. *Nature* 464:864–869.
28. McMahon HT, Gallop JL (2005) Membrane curvature and mechanisms of dynamic cell membrane remodeling. *Nature* 438:590–596.
29. Zimmerberg J, Kozlov MM (2006) How proteins produce cellular membrane curvature. *Nat Rev Mol Cell Biol* 7:9–19.
30. Ford MG, et al. (2002) Curvature of clathrin-coated pits driven by epsin. *Nature* 419:361–366.
31. Martens S, Kozlov MM, McMahon HT (2007) How synaptotagmin promotes membrane fusion. *Science* 316:1205–1208.
32. Peter BJ, et al. (2004) BAR domains as sensors of membrane curvature: The amphiphysin BAR structure. *Science* 303:495–499.
33. Hu J, et al. (2008) Membrane proteins of the endoplasmic reticulum induce high-curvature tubules. *Science* 319:1247–1250.
34. Young JD, Podack ER, Cohn ZA (1986) Properties of a purified pore-forming protein (perforin 1) isolated from H-2-restricted cytotoxic T cell granules. *J Exp Med* 164:144–155.
35. Baran K, et al. (2009) The molecular basis for perforin oligomerization and transmembrane pore assembly. *Immunity* 30:684–695.
36. Keefe D, et al. (2005) Perforin triggers a plasma membrane-repair response that facilitates CTL induction of apoptosis. *Immunity* 23:249–262.
37. Thiery J, et al. (2010) Perforin activates clathrin- and dynamin-dependent endocytosis, which is required for plasma membrane repair and delivery of granzyme B for granzyme-mediated apoptosis. *Blood* 115:1582–1593.
38. Mathivet L, Cribier S, Devaux PF (1996) Shape change and physical properties of giant phospholipid vesicles prepared in the presence of an AC electric field. *Biophys J* 70:1112–1121.
39. Majhenc J, Bozic B, Svetina S, Zeks B (2004) Phospholipid membrane bending as assessed by the shape sequence of giant oblate phospholipid vesicles. *Biochim Biophys Acta* 1664:257–266.
40. Morales-Penningston NF, et al. (2010) GUV preparation and imaging: Minimizing artifacts. *Biochim Biophys Acta* 1798:1324–1332.
41. Chernomordik LV, Zimmerberg J (1995) Bending membranes to the task: Structural intermediates in bilayer fusion. *Curr Opin Struct Biol* 5:541–547.
42. Yamaji-Hasegawa A, et al. (2003) Oligomerization and pore formation of a sphingomyelin-specific toxin, lysenin. *J Biol Chem* 278:22762–22770.
43. Bonev BB, Gilbert RJC, Andrew PW, Byron O, Watts A (2001) Structural analysis of the protein/lipid complexes associated with pore formation by the bacterial toxin pneumolysin. *J Biol Chem* 276:5714–5719.
44. Farsad K, et al. (2001) Generation of high curvature membranes mediated by direct endophilin bilayer interactions. *J Cell Biol* 155:193–200.
45. Solon J, Gareil O, Bassereau P, Gaudin Y (2005) Membrane deformations induced by the matrix protein of vesicular stomatitis virus in a minimal system. *J Gen Virol* 86:3357–3363.
46. Lamaziere A, et al. (2007) Non-metabolic membrane tubulation and permeability induced by bioactive peptides. *PLoS One* 2:e201.
47. Reynwar BJ, et al. (2007) Aggregation and vesiculation of membrane proteins by curvature-mediated interactions. *Nature* 447:461–464.
48. Watkins EB, Miller CE, Majewski J, Kuhl TL (2011) Membrane texture induced by specific protein binding and receptor clustering: Active roles for lipids in cellular function. *Proc Natl Acad Sci USA* 108:6975–6980.
49. Tilley SJ, Orlova EV, Gilbert RJC, Andrew PW, Saibil HR (2005) Structural basis of pore formation by the bacterial toxin pneumolysin. *Cell* 121:247–256.
50. Froelich CJ, Turbov J, Hanna W (1996) Human perforin: Rapid enrichment by immobilized metal affinity chromatography (IMAC) for whole cell cytotoxicity assays. *Biochem Biophys Res Commun* 229:44–49.
51. Gilbert RJC, et al. (1999) Studies on the structure and mechanism of a bacterial protein toxin by analytical ultracentrifugation and small-angle neutron scattering. *J Mol Biol* 293:1145–1160.
52. Bruhn H, Winkelmann J, Andersen C, Andrä J, Leippe M (2006) Dissection of the mechanisms of cytolytic and antibacterial activity of lysenin, a defence protein of the annelid *Eisenia fetida*. *Dev Comp Immunol* 30:597–606.
53. Peterlin P, Arrigler V (2008) Electroformation in a flow chamber with solution exchange as a means of preparation of flaccid giant vesicles. *Colloids Surf B* 64:77–87.
54. Dalla Serra M, Menestrina G (2000) Characterization of molecular properties of pore-forming toxins with planar lipid bilayers. *Methods Mol Biol* 145:171–188.